Photon dominated regions in the spiral arms of M 83 and M 51

Carsten Kramer, Bhaswati Mookerjea, Estelle Bayet, Santiago García-Burillo, Maryvonne Gerin, Frank P. Israel, J. Stutzki, J. G. A. Wouterloot

A&A 441, 961–973 (2005)
DOI: 10.1051/0004-6361:20053358

Astronomy & Astrophysics

Photon dominated regions in the spiral arms of M 83 and M 51⋆

C. Kramer[1], B. Mookerjea[1], E. Bayet[2], S. Garcia-Burillo[3], M. Gerin[2], F. P. Israel[4], J. Stutzki[1], and J. G. A. Wouterloot[5]

[1] KOSMA, I. Physikalisches Institut, Universität zu Köln, Zülpicher Straße 77, 50937 Köln, Germany
e-mail: kramer@ph1.uni-koeln.de
[2] Radioastronomie Millimétrique: UMR 8540 du CNRS, Laboratoire de Physique de l'ENS, 24 rue Lhomond, 75231 Paris Cedex 05, France
[3] Centro Astronomico de Yebes, IGN, 19080 Guadalajara, Spain
[4] Sterrewacht Leiden, PO Box 9513, 2300 RA Leiden, The Netherlands
[5] Joint Astronomy Centre, 660 N. A'ohoku Place, 96720 Hilo, HI, USA

Received 3 May 2005 / Accepted 2 June 2005

ABSTRACT

We present [C I] $^3P_1$–$^3P_0$ spectra at four spiral arm positions and the nuclei of the nearby galaxies M 83 and M 51 obtained at the JCMT. The spiral arm positions lie at galacto-centric distances of between 2 kpc and 6 kpc. This data is complemented with maps of CO 1–0, 2–1, and 3–2, and ISO/LWS far-infrared data of [C II] (158 μm), [O I] (63 μm), and [N II] (122 μm) allowing for the investigation of a complete set of all major gas cooling lines. From the intensity of the [N II] line, we estimate that between 15% and 30% of the observed [C II] emission originates from the dense ionized phase of the ISM. The analysis indicates that emission from the diffuse ionized medium is negligible. In combination with the FIR dust continuum, we find gas heating efficiencies below ~0.21% in the nuclei, and between 0.25 and 0.36% at the outer positions. Comparison with models of photon-dominated regions (PDRs) with the standard ratios [O I](63)/[C II]$_{\rm PDR}$ and ([O I](63)+[C II]$_{\rm PDR}$) vs. TIR, the total infrared intensity, yields two solutions. The physically most plausible solution exhibits slightly lower densities and higher FUV fields than found when using a full set of line ratios, [C II]$_{\rm PDR}$/[C I](1–0), [C I](1–0)/CO(3–2), CO(3–2)/CO(1–0), [C II]/CO(3–2), and, [O I](63)/[C II]$_{\rm PDR}$. The best fits to the latter ratios yield densities of 10^4 cm^{-3} and FUV fields of ~G_0 = 20–30 times the average interstellar field without much variation. At the outer positions, the observed total infrared intensities are in agreement with the derived best fitting FUV intensities. The ratio of the two intensities lies at 4–5 at the nuclei, indicating the presence of other mechanisms heating the dust. The [C I] area filling factors lie below 2% at all positions, consistent with low volume filling factors of the emitting gas. The fit of the model to the line ratios improves significantly if we assume that [C I] stems from a larger region than CO 2–1. Improved modelling would need to address the filling factors of the various submm and FIR tracers, taking into consideration the presence of density gradients of the emitting gas by including cloud mass and size distributions within the beam.

Key words. galaxies: ISM – galaxies: structure – galaxies: individual: M 83, M 51 – ISM: structure – infrared: galaxies – submillimeter

1. Introduction

Neutral atomic carbon is thought to form predominantly in surface layers of molecular clouds where C II recombines and CO is dissociated due to the far-UV photons governing the chemical reactions. FUV photons (6 eV < $h\nu$ < 13.6 eV) are primarily responsible for the heating of the surface regions via the photoelectric effect on dust grains while at larger depth cosmic-ray induced heating will dominate. These regions are referred to as photo dissociation regions or, more generally, as photon dominated regions (PDRs) (Tielens & Hollenbach 1985; Stoerzer et al. 1996; Kaufman et al. 1999). PDR models take into account the relevant physical processes, and solve simultaneously for the chemistry (using an extensive chemical network) and the thermal balance, as a function of cloud depth. It is found that the ratio of [C II]/[C I] is an accurate tracer of the FUV field (Gerin & Phillips 2000), parametrized by G_0 in units of the Habing-field 1.6×10^{-3} erg s^{-1} cm^{-2} (Habing 1968). Another important parameter governing the depth at which C I forms is the ratio of density over FUV field n/G_0 (Tielens & Hollenbach 1985). This ratio also determines the efficiency of converting FUV photons to gas heating, i.e. the photoelectric heating efficiency ϵ (Bakes & Tielens 1994).

While the Milky Way survey of FIR lines conducted with COBE/FIRAS (Fixsen et al. 1999) showed that [C II] is the dominant cooling line, it also showed the importance of the two finestructure lines of [C I]. Both lines are ubiquitous and the two lines together amount to 75% of the total cooling of all rotational CO lines in the inner galaxy. This picture has also emerged from extragalactic observations of the [C I] 1–0 line.

⋆ Figure 4 is only available in electronic form at http://www.edpsciences.org

These show again that the cooling due to C I and CO are of the same order of magnitude for most galaxies (Bayet et al. 2004; Israel & Baas 2003, 2002, 2001). C I is found to be a good tracer of molecular gas, possibly more reliable than CO (Gerin & Phillips 2000).

Several coordinated mapping studies of nearby galaxies have been started during the past years. The BIMA SONG survey (Regan et al. 2001) has aimed at obtaining the ^{12}CO emission of 1–0 and 2–1 rotational lines at high spatial resolutions. There exist velocity-integrated [C II] observations of large samples of galaxies at ∼1′ resolution with the KAO (Stacey et al. 1991) and with ISO (Malhotra et al. 2001), hereafter MKH01, and (Leech et al. 1999; Negishi et al. 2001). The SINGS Spitzer Legacy Project (Kennicutt et al. 2003) has started imaging 75 galaxies in the infrared, including M 51. In the coming years, both SOFIA and the Herschel Space Observatory are expected to provide velocity-resolved [C II] data at resolutions of ∼10″, complementary to many current single dish observations of CO and [C I].

In external galaxies where a large number of clouds or even GMCs fill the beam it is difficult to seperate the different contributions and judge their importance. A long standing problem is that a substantial fraction of the [C II] emission may originate from the diffuse ionized and neutral medium. Comparison with [N II] helps to estimate the fraction originating from PDRs, but usually with large uncertainties due to the varying chemical and excitation conditions in different galactic environments (e.g. Contursi et al. 2002). The present study is part of the preparatory work for future airborne and space missions like SOFIA and Herschel. In addition, it may serve as a template for studies of e.g. [C I] and CO in high-z galaxies which have recently become possible (Weiss et al. 2005; Walter et al. 2004; Pety et al. 2004; Neri et al. 2003; Weiss et al. 2003).

Most extragalactic observations of atomic carbon have so far concentrated on the bright galactic nuclei or enhanced emission of edge-on galaxies. Here, we compare observations of the two nuclei of M 83 and M 51 with pointed observations at spiral arm positions which show enhanced star forming activity. The galacto-centric distances of the selected outer positions lie between 1.8 and 5.8 kpc. We combine observations of atomic carbon with low and mid-J CO and ^{13}CO data, as well as FIR [C II], [O I](63 μm), and [N II](122 μm) data from the ISO database and thus include the brightest gas cooling lines of the far-infrared and submillimeter regime.

1.1. M 83

M 83 (NGC 5236) is the most nearby CO-rich grand-design spiral galaxy, seen almost face-on (Table 1). It has a pronounced bar, with two well-defined spiral arms connected to the starburst nucleus. In this paper, we adopt a distance of 3.7 Mpc (de Vaucouleurs et al. 1991), though recent observations of Cepheids indicate a slightly larger distance of 4.5 Mpc (Thim et al. 2003).

Low-J CO maps were obtained by Crosthwaite et al. (2002), Lundgren et al. (2004b,a), Dumke et al. (2001) and Sakamoto et al. (2004). [C I] observations of the center were conducted by Israel & Baas (2002) and Petitpas & Wilson (1998). Pointed KAO observations report strong FIR fine-structure lines towards the nucleus with a rapid fall-off towards the arms (Crawford et al. 1985).

Table 1. Basic properties of M 83 and M 51. $D_{25} \times d_{25}$ is the optical diameter from the RC3 catalogue. $L_{\rm FIR}$ is the surface integrated far-infrared luminosity between 42.5 and 122.5 μm using the listed distance. F_{60}/F_{100} is the IRAS color ratio of the surface integrated flux densities at 60 μm and 100 μm, corrected for extinction.

	M 83	M 51
RA(2000)	13:37:00.5	13:29:52.7
Dec(2000)	−29:51:55.3	47:11:43
Type	SAB(s)c[(1)]	SA(s)bc pec[(1)]
Distance [Mpc]	3.7[(5)]	9.6 [(4)]
10″ correspond to	179 pc	465 pc
Heliocentric velocity [km s^{-1}]	516[(1)]	463[(1)]
Position Angle [deg]	45 [(2)]	170
Inclination [deg]	24 [(2)]	20
$D_{25} \times d_{25}$ [′]	12.9×11.5[(1)]	11.2×6.9[(1)]
$L_{\rm FIR}$ [10^9 $L_\odot$]	7.1[(3)]	14[(3)]
F_{60}/F_{100}	0.43[(3)]	0.44[(3)]
F_{60} [Jy]	286[(3)]	85[(3)]

References: (1) RC3 catalogue (de Vaucouleurs et al. 1991); (2) Talbot et al. (1979), Tully (1988); (3) Rice et al. (1988); (4) Sandage & Tammann (1975); (5) de Vaucouleurs (1979).

Here, we present new [C I] data of the center and two spiral arm positions on the north-eastern arm and south-western bar-spiral transition zone. The emission of [C II], [N II](122), and [O III](88) observed with ISO/LWS (Brauher 2005, priv. comm.) is strongly enhanced in these interface regions, indicating greatly enhanced star formation rates. ISO/LWS emission from the center was analyzed by Negishi et al. (2001). The north-eastern arm was previously studied by Lord & Kenney (1991) and Rand et al. (1999) who presented OVRO interferometric ^{12}CO 1–0 maps. The eastern position at (89″, 38″) presented here corresponds to the bright feature #6 discussed by Rand et al. (1999, Table 4). About 15″ to the east of the CO arm newly formed stars form the optical arm and an HI ridge. At #6, the CO and dust arms coincide while they are offset further to the south. Position (−80″, −72″) studied here corresponds to a CO 1–0 peak in the south-western bar-spiral transition zone which exhibits a massive GMC complex and luminous H II regions (Kenney & Lord 1991). Note that only less than 5% of the single dish flux is recovered by the interferometric maps (Rand et al. 1999). Thus, relatively smoothly distributed diffuse molecular gas is completely missed.

1.2. M 51

The nearby grand-design spiral galaxy M 51 (NGC 5194) seen almost face on (Table 1) is interacting with its small companion NGC 5195, which lies 4.5′ to the north. M 51 is a Seyfert 2 galaxy (Ho et al. 1997). The central AGN is surrounded by a ∼100 pc disk (Kohno et al. 1996) of dense and warm gas (Matsushita et al. 1998).

Table 2. Overview of the [C I], CO, and ^{13}CO data of M 83 and M 51. θ_b is the telescope half power beamwidth. All spectra are scaled to main beam brightness temperatures, $T_{mb} = T_A^*/\eta_{mb}$.

Line	θ_b ($''$)	Telescope	η_{mb}	Refs.	
M 83 at (0, 0), (89, 38), (−80, −72)					
[C I] 1–0	10	JCMT 15 m	0.52	1	point.
CO 1–0	21	IRAM 30 m	0.78	1	point.
CO 1–0	55	NRAO 12 m	0.88	2	map
CO 2–1	10	IRAM 30 m	0.57	1	point.
CO 2–1	28	NRAO 12 m	0.56	2	map
CO 3–2	25	CSO 10 m	0.75	3	map
^{13}CO 1–0	22	IRAM 30 m	0.79	1	point.
^{13}CO 2–1	10	IRAM 30 m	0.60	1	point.
M 51 at (0, 0), (72, 84), (−84, −84)					
[C I] 1–0	10	JCMT 15 m	0.52	1	point
CO 1–0	21	IRAM 30 m	0.65	5	map
CO 2–1	10	IRAM 30 m	0.46	5	map
CO 3–2	22	HHT 10 m	0.50	4	map
^{13}CO 1–0	22	IRAM 30 m	0.79	1	point.
^{13}CO 2–1	10	IRAM 30 m	0.60	1	point.

References: 1: new data for this paper; 2: Crosthwaite et al. (2002); 3: Bayet et al. (priv. comm.); 4: Wielebinski et al. (1999), Nieten et al. (1999), Dumke et al. (2001); 5: Garcia-Burillo et al. (1993b). The last column indicates whether single pointings or maps are available. The mapped CO data was Gauss-smoothed to the 80″ ISO/LWS resolution.

A large amount of observational data are available for this object, including an extended KAO map of [C II] (Nikola et al. 2001). Garnett et al. (2004) used ISO/LWS data of the M 51 H II region CCM 10 to study the ionized gas, finding that abundances are roughly solar.

Several single-dish studies mapped the low-lying rotational ^{12}CO and ^{13}CO transitions. CO 1–0 and 2–1 was mapped by Garcia-Burillo et al. (1993a,b) and Nakai et al. (1994); Tosaki et al. (2002). In this grand-design spiral, CO is tightly confined to the spiral arms. Maps of CO 3–2 and 4–3 were obtained at the HHT by Nieten et al. (1999), Wielebinski et al. (1999), and Dumke et al. (2001) who show that warm molecular gas is extended in M 51 at galacto-centric distances of at least up to 100″, resp. 5 kpc. Single-dish observations of neutral carbon were so far obtained only in the center region by Gerin & Phillips (2000); Israel & Baas (2002), and Israel et al. (2005, in prep.).

Aperture synthesis maps were obtained by Aalto et al. (1999); Sakamoto et al. (1999) and Regan et al. (2001) in CO 1–0 at resolutions of 4″−6″. Recently, Matsushita et al. (2004) mapped the inner region in ^{12}CO 3–2.

Here, we selected two spiral arm positions lying in the northeastern and the southwestern zones, i.e. at 72″, 84″ and −84″, −84″, of enhanced [C II] emission tracing enhanced star formation (Nikola et al. 2001). ISO/LWS data are available for these positions, and for the center (Negishi et al. 2001; and Brauher 2005, priv. comm.). The H II region studied by Garnett et al. (2004) using ISO/LWS, CCM 10, lies at about +148″, +45″ (Carranza et al. 1969), 1.5′ to the north-west of 72″, 84″.

2. Data sets

We present here observations of [C I], CO, and ^{13}CO spectra at four spiral arm positions and the centers of M 51 and M 83 (Table 2). We combine these with ISO/LWS FIR spectral line data at all six positions together with the FIR continuum derived from HIRES/IRAS 60 μm and 100 μm maps.

2.1. [C I] data taken at the JCMT

We have observed the fine structure transition of atomic carbon ([C I]) at 492 GHz (609 μm, $^3P_1-^3P_0$; hereafter 1−0) in M 51 (3 positions) and M 83 (3 positions) using the JCMT 15m telescope. We used the RxW receiver with a single mixer and the DAS autocorrelator. Observations were carried out over 35 h in May and June 2003. We used the double-beamswitch observing mode with a wobbler throw of ±3′ in the direction of the major axis, i.e. in the direction of the largest velocity gradient. Pointing was checked using SCUBA after an initial alignment with RxW and Jupiter at the start of each shift. It was found to be accurate to within 2−3″. The atmospheric zenith opacity at 225 GHz varied slowly between 0.1 and 0.05, corresponding to a τ of 2 and 1 at 492 GHz. After merging the DAS autocorrelator spectra using the SPECX software, further data analysis was done using the CLASS/GILDAS package of IRAM.

2.2. CO data taken at the IRAM 30 m MRT

We have observed the ^{12}CO and ^{13}CO 1–0 and 2–1 rotational transitions at all six positions in M 51 and M 83 using the IRAM 30 m telescope. These observations were carried out in double beam switch mode with a wobbler throw of ±4′ using the filterbank of 1 MHz resolution for the 3 mm band and the 4 MHz filterbank for the 1 mm band. Observations were carried out over 15 h on July, 23rd and 26th, and on September, 10th, 2004. Pointing and focus were checked and corrected every ∼2 h. The pointing accuracy was better than 4″. The amount of precipitable water vapour varied slowly between 10 and ∼20 mm. Telescope parameters are listed in Table 2.

2.3. FIR line fluxes from ISO/LWS

The central area of M 83 covering ∼5′ × 4′ was mapped on a fully-sampled grid of 61 positions with ISO/LWS. M 51 was observed at 13 positions, mainly along a cut through the center and the two prominent [C II] lobes in the north-east and south-west seen in the KAO map by Nikola et al. (2001). The ISO/LWS line emission data was uniformly processed by Brauher (2005, priv. comm.) to derive line fluxes in Wm^{-2}. To convert to intensities, we use a LWS beam size of 80″ ($\Omega_{LWS} = 1.2 \times 10^{-7}$ sr), the mean value published in the latest LWS Handbook, and extended source corrections factors (Gry et al. 2003). Resulting ISO intensities of [C II] (158 μm, [N II] (122 μm), and [O I] (63 μm) at the positions observed in [C I] are listed in Table 3. Since the [O I] (146 μm) line was detected only at the center positions (S. Lord, priv. comm.), we did not include it in the present analysis.

Table 3. FIR continuum and line intensities in units of 10^{-6} erg s^{-1} cm^{-2} sr^{-1}. The absolute calibration error is assumed to be 15% (Gry et al. 2003).

Positions ($\Delta\alpha, \Delta\delta$) ($''$, $''$)	HIRES FIR	ISO/LWS [C II] 158 μm	[N II] 122 μm	[O I] 63 μm
M 83:				
(0, 0)	32×10^3	81.8	14.1	86.7
(–80, –72)	7.2×10^3	38.6	5.3	27.3
(89, 38)	6.6×10^3	33.4	5.9	26.6
M 51:				
(0,0)	17×10^3	44.1	12.3	32.2
(72, 84)	4.6×10^3	16.7	<2.3	13
(–84, –84)	3.5×10^3	15.4	2.1	13.4

2.4. FIR continuum maps taken with IRAS

To derive the far-infrared continuum at all selected positions, we obtained high-resolution (HIRES) 60 μm and 100 μm IRAS maps from the IPAC data center[1]. Enhanced resolution images were created after 200 iterations using the maximum correlation method (MCM Aumann et al. 1990). These data were smoothed to an effective common circular beam of 80″ and then combined to create maps of the far-infrared flux. The FIR flux is defined as in Helou et al. (1988): FIR = $1.26 \times 10^{-14}[2.58\, I(60\,\mu\text{m}) + I(100\,\mu\text{m})]$ where FIR is in W m^{-2} and I is in Janskys. FIR is a good estimate of the flux contained between 42.5 and 122.5 μm (Helou et al. 1988). Table 3 lists the FIR flux at the selected positions. To derive the total infrared flux TIR, we follow the procedure introduced by Dale et al. (2001) who derived an analytical expression for the ratio of total infrared flux TIR to the observed FIR flux, i.e. the bolometric correction, as a function of the 60 μm/100 μm flux density ratio from modelling the infrared SEDs of 69 normal galaxies[2] For M 83 and for M 51, the total infrared flux is a factor 2.3 larger than FIR given the global 60 μm/100 μm ratio of 0.43 (Table 1).

3. Spectra and line ratios

The main aim of this work is to use the combined FIR ISO/LWS, HIRES/IRAS, and the millimeter/submillimeter line data coherently and to investigate to what degree these give a consistent fit within the framework of a simple model scenario such as PDR excitation. We therefore smoothed the ^{12}CO maps (Table 2) to the ISO/LWS angular resolution of 80″ using Gaussian kernels. Spectra of [C I], CO, and ^{13}CO are displayed in Figs. 1, 2 and integrated intensities in Table 4. Ratios with [C I] and ^{13}CO for which no maps exist were corrected for beam filling (Table 5).

[1] A description of IRAS HiRes reduction is available at `http://irsa.ipac.caltech.edu/IRASdocs/hires_over.html`

[2] Note that TIR corresponds to the bolometric FIR dust continuum emission I(FIR) used in the PDR models of Kaufman et al. (1999).

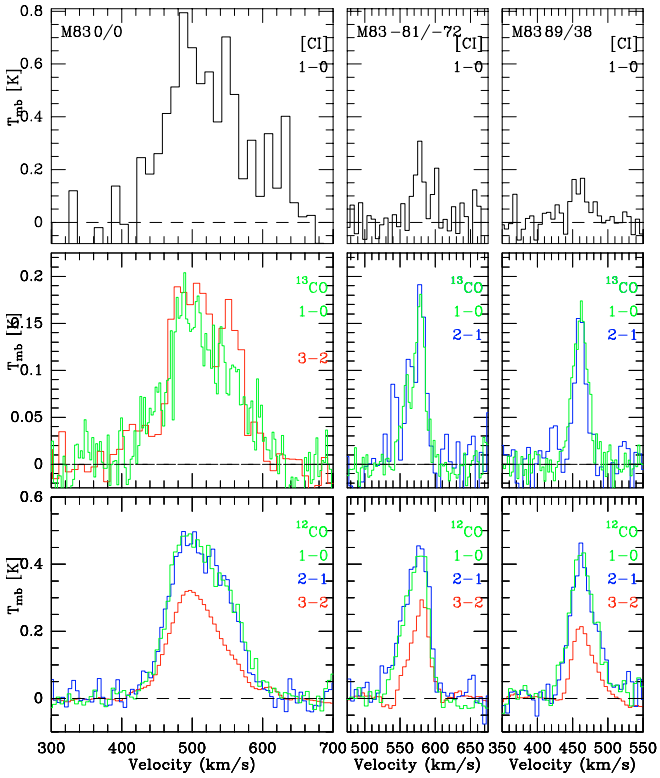

Fig. 1. Spectra of M 83 at the central and two spiral arm positions (Table 2). Offsets are given in arcseconds relative to the (0, 0) position (Table 1). Velocities are relative to LSR. All spectra are on the T_{mb} scale. The ^{12}CO data are at a common resolution of 80″. The [C I] and ^{13}CO data are at their original resolutions listed in Table 2.

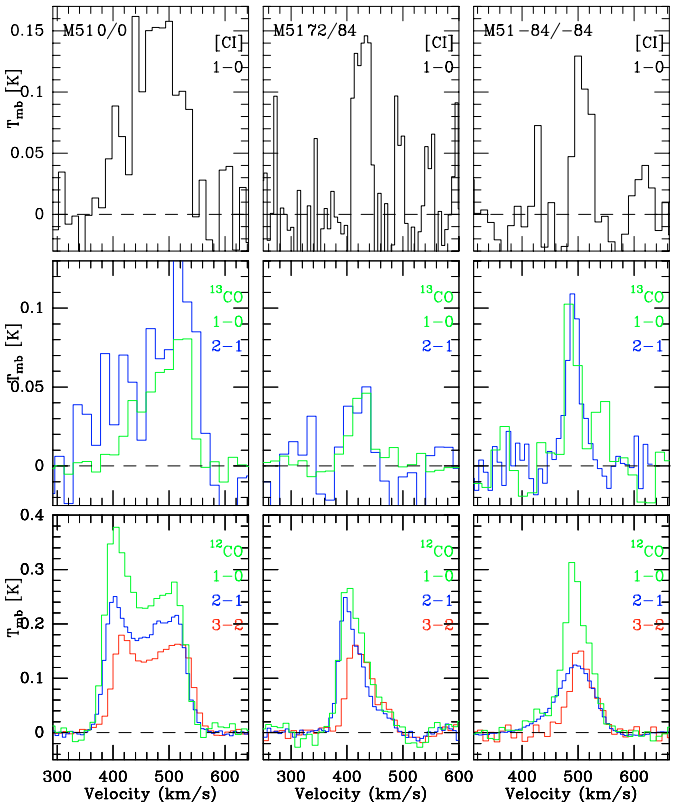

Fig. 2. Spectra of M 51 at the central and two spiral arm positions (cf. Fig. 1).

Table 4. Integrated intensities in K km s^{-1} (all columns but Cols. 1, 2 and 4) at the resolutions used for the spectra in Figs. 1, 2. Column 2 gives galacto-centric distances R_{gal} in kpc. The calibration error is estimated to be ∼15%. (The observed [C I] intensities at the center positions agree within 20% with previous data presented in Gerin & Phillips 2000; and Petitpas & Wilson 1998.) Column 4 lists [C I] luminosities in K km s^{-1} kpc^2 in brackets, i.e. the intensities integrated over the 10″ JCMT beam.

($\Delta\alpha$,$\Delta\delta$)	R_{gal}	[CI]		CO 1–0	CO 2–1	CO 3–2	^{13}CO 1–0	^{13}CO 2–1
		HPBW = 10″		80″	80″	80″	22″	10″
(1)	(2)	(3)	(4)	(5)	(6)	(7)	(8)	(9)
M 83:								
(0, 0)	0	79.55	(2)	50.63	47.03	30.15	19.36	21.33
(–80, –72)	1.93	7.57	(0.19)	18.17	18.06	8.35	4.6	5.1
(89, 38)	1.76	4.53	(0.11)	17.03	15.93	7.84	4.28	3.27
M 51:								
(0, 0)	0	16.36	(2.78)	43.42	31.53	23.68	7.34	12.65
(72, 84)	5.4	4.59	(0.78)	15.32	12.21	9.19	2.27	1.43
(–84, –84)	5.77	4.03	(0.69)	17.29	9.85	7.41	4.01	3.09

Table 5. Line ratios of integrated intensities in K km s^{-1}. The 1σ errors are ∼21%. The CO 3–2/1–0 ratio was added to allow an easier comparison with the literature. To compare all data at a common resolution of 80″, we scaled the [C I] and ^{13}CO data, for which maps are not available, using the beam filling factors $\Phi_B^{80/10}$ and $\Phi_B^{80/21}$. The factor $\Phi_B^{80/10}$ for [C I] and ^{13}CO 2–1 data was derived from the ratio of ^{12}CO 2–1 integrated intensities at 80″ and at 10″ resolution. Likeweise, the factor $\Phi_B^{80/21}$ for ^{13}CO 1–0 data was derived from CO 1–0.

$\Delta\alpha, \Delta\delta$	$\Phi_B^{80/10}$	$\Phi_B^{80/21}$	CO 3–2 / CO 1–0	CO 3–2 / CO 2–1	CO 2–1 / CO 1–0	CO 1–0 / ^{13}CO 1–0	CO 2–1 / ^{13}CO 2–1	[C I] 1–0 / ^{13}CO 2–1	[C I] 1–0 / CO 3–2
[″, ″]									
M 83:									
(0, 0)	0.22	0.28	0.6	0.64	0.93	9.34	10.02	3.73	0.58
(–80, –72)	0.37	0.45	0.46	0.46	0.99	8.77	9.58	1.48	0.34
(89, 38)	0.48	0.47	0.46	0.49	0.93	8.46	10.14	1.38	0.28
M 51:									
(0, 0)	0.56	0.68	0.55	0.76	0.73	8.31	4.62	1.4	0.4
(72, 84)	0.62	0.73	0.6	0.76	0.8	9.27	13.81	3.19	0.3
(–84, –84)	0.52	0.72	0.43	0.75	0.57	6.04	6.09	1.25	0.27

3.1. M 83

The [C I] lines are widest at the center position with 130 km s^{-1} *FWHM* and drop to about 30 km s^{-1} at the two outer positions. In addition, peak line temperatures drop strongly, leading to a pronounced drop of [C I] integrated intensities and area integrated [C I] luminosities by factors of 10 to 18 at galacto-centric distances of less than 2 kpc (Table 4).

The CO 3–2 transition traces warm and dense gas since its upper level energy corresponds to 2.8 $J(J+1) = 33.6$ K and the critical density needed to thermalize this line is $4 \times 10^3\, J^3 \sim 1 \times 10^5$ cm^{-3}, only weakly dependent on the kinetic temperature. Trapping typically reduces the critical densities by up to an order of magnitude, depending on the optical depth of the lines. The CO 3–2/1–0 line ratio of integrated intensities (Table 5) thus is a sensitive tracer of local densities for densities of less than ∼10^5 cm^{-3}. Here, both line maps were smoothed to 80″ resolution, beam filling factors thus cancel out to first order. The estimated calibration error is 21%. While the 2–1/1–0 ratio is ∼1 at all positions indicating that the $J = 2$ state is thermalized, the 3–2/1–0 ratio drops slightly from 0.60 in the center to 0.46 at the spiral arm positions. These ratios indicate that densities are lower than 1×10^5 needed for thermalization of the $J = 3$ level.

The ^{12}CO 2–1 vs. ^{13}CO 2–1 line ratio, as well as the corresponding 1–0 ratio, trace the total column densities of the ^{13}CO line. The ratios remain constant at ∼10 for 2–1 and ∼9 for the 1–0 transition.

The above ratios found at the center position agree within the quoted errors with the ratios presented in Israel & Baas (2001).

In M 83, we find a significant drop of the CI vs. ^{13}CO 2–1 ratio from about 4 in the center to ∼1.4 at the two outer positions.

3.2. M 51

Again, the [C I] line is widest at the center, ∼100 km s^{-1} *FWHM*, and drops to ∼30 km s^{-1} at the two outer positions. The ^{13}CO lines show similar line widths at all three positions. Peak temperatures of [C I] hardly drop between the center and the two outer positions. Resulting integrated intensities and luminosities drop by a factor of ∼4 only.

Table 6. Results of the escape probability analysis using the four observed line ratios ^{12}CO 3–2/2–1, ^{12}CO 2–1/1–0, ^{12}CO/^{13}CO 1–0, and 2–1. N(CO) is the total CO column density per 80″ beam. M is the total mass integrated over the beam and assuming an abundance ratio of [CO]/[H$_2$] = 8.5×10^{-5} (Frerking et al. 1982). $n_{\rm av}$ is the average density assuming that emission stems from a sphere with beam diameter.

$\Delta\alpha/\Delta\delta$ [″, ″]	$\chi^2_{\rm min}$	$n_{\rm loc}$ [cm^{-3}]	$T_{\rm kin}$ [K]	N(CO)/Δv [10^{16} cm^{-2}/km s^{-1}]	N(CO) [10^{16} cm^{-2}]	M [10^6 $M_\odot$]	$n_{\rm av}$ [cm^{-3}]
M 83:							
(0, 0)	1.7	3000.	15.0	3.2	15.79	65.16	0.42
(−80, −72)	3.5	3000.	12.5	3.2	7.58	31.29	0.20
(89, 38)	2.1	3000.	12.5	3.2	6.69	27.60	0.18
M 51:							
(0, 0)	3.6	30000.	12.5	3.2	17.41	484.67	0.18
(72, 84)	4.0	3000.	15.0	3.2	2.07	57.76	0.02
(−84, −84)	7.4	10000.	12.5	3.2	5.46	151.89	0.06

The observed CO 2–1/1–0 ratios lie between 0.6 and 0.8 for all three positions and do not peak at the center. This indicates that not even the 2–1 line is thermalized in M 51. However, the CO 3–2/2–1 ratios do not drop as would be expected but equal the CO 2–1/1–0 ratio or even exceed them, while staying below 0.8. This is difficult to explain with a single component model as we will show below. The center CO 3–2/1–0 ratio of 0.55 is in agreement with ratios previously found with single-dish telescopes which range between 0.5−0.8 at beam sizes of ∼14″ to 24″ (Matsushita et al. 1999; Mauersberger et al. 1999; Wielebinski et al. 1999). Interferometric observations at ∼4″ resolution tracing the dense nuclear gas show a high 3–2/1–0 ratio of 1.9 Matsushita et al. (2004).

High central column densities are indicated in this work by the rather low ^{12}CO/^{13}CO 2–1 ratio of 4.6. In contrast, the outer postions show ratios between 6 and 14.

We find CI vs. ^{13}CO 2–1 ratios of ∼1 at the center and at (−84, −84) while (72, 84) exhibits a high ratio of 3.2.

3.3. Comparison

The gradients of [C I] luminosities with galacto-centric distances are strikingly different in M 51 and M 83. M 83 is much more centrally peaked, [C I] luminosities drop by a factor of 18 at only 1.8 kpc distance in M 83. In contrast, luminosities in M 51 drop by only a factor of 4 at galacto-centric distances which are more than a factor of 3 larger, i.e. at 5.8 kpc. However, the central [C I] luminosities of M 51 and M 83 agree within 40%.

The line widths observed at the outer positions of M 51 and M 83 are typical for the disks of these two galaxies (Handa et al. 1990; Garcia-Burillo et al. 1992). See Table 2 of Garcia-Burillo et al. (1993a) for a compilation of CO line widths found in these and several other galaxies.

The CI vs. ^{13}CO 2–1 ratio in the Milky Way is often found to be 1 (e.g. Keene 1995) while Israel (2005); Israel & Baas (2002) find a strong variation of this ratio for 15 galactic nuclei. The [C I] line is stronger than the ^{13}CO 2–1 line for all but three galaxy centers. The highest ratios are about 5. Here, we find a variation between 1.3 and 4.

For galaxy centers, Israel & Baas (2002) found that this ratio is well correlated with the [C I] luminosity covering a range of 160 K km s^{-1} kpc^2 in the active nucleus of NGC 3079 down to ∼1 K km s^{-1} kpc^2 in the quiescent center of Maffei 2. Here, we increase the range down to 0.11 K km s^{-1} kpc^2 (Table 4) at the same resolution of 10″. In contrast to the galaxy centers, the spiral arm positions observed here do not show a systematic correlation between the [C I]/^{13}CO line ratio and [C I] luminosity.

4. Physical conditions

4.1. Simple homogeneous models

As shown above, the observed CO line ratios cannot be explained with a simple LTE analysis. As a first step in order to estimate the kinetic temperatures and local densities of the CO emitting gas, we present in this section the results of slightly more realistic escape probability radiative transfer calculations of homogeneous spherical clumps (Stutzki & Winnewisser 1985). We assumed a ^{12}CO/^{13}CO abundance ratio of 40 (Mauersberger & Henkel 1993). As input, we use the four ratios of integrated intensities (Table 5): ^{12}CO 3–2/2–1, ^{12}CO 2–1/1–0, ^{12}CO/^{13}CO 1–0, and ^{12}CO/^{13}CO 2–1. We calculated model intensities of the three transitions for column densities $10^{14} < N({\rm CO})/\Delta v/({\rm cm^{-2}/(K\,km\,s^{-1})}) < 10^{22}$, local H$_2$ densities $10 < n_{\rm loc}/{\rm cm^{-3}} < 40$, and kinetic temperatures $10 < T_{\rm kin}/{\rm K} < 40$. The modelled ratios were compared with the observed ratios taking into account the observational error of 21% to derive the χ^2. The best fitting N(CO)/Δv, n, and $T_{\rm kin}$ together with the corresponding minimum reduced χ^2 are listed in Table 6.

Below, we first describe the results of the one-component fits for the positions observed in M 83 and M 51. Much more complete physical models of the emitting regions are presented in the next Sect. 4.2.

M 83: at 80″ resolution, the ^{12}CO line ratios do not vary significantly between the center and the two bright spiral arm positions observed here. A ^{12}CO 3–2/1–0 ratio of 0.5 indicates an excitation temperature of ∼10 K assuming optically thick thermalized emission and simply using the detection equation.

The escape probability analysis leads to a similar result (Table 6). At all three positions, the ratios are well modelled by a one-component model with a rather low kinetic temperature of only 12−15 K and a density of $n_{\rm loc} = 3 \times 10^3\,{\rm cm}^{-3}$. This result does not exclude the existence of a warmer and denser gas phase as would be traced by higher CO transitions or the 63 μm [O I] line as discussed below. For the center, Israel & Baas (2001) have in fact deduced a warmer phase by including observations of the CO 4–3 line in their radiative transfer analysis.

The ^{12}CO and ^{13}CO line ratios found in M 83 are characteristic for dynamically active or starburst regions in the classification scheme of Papadopoulos et al. (2004). In this scheme, extreme starbursts would show similar ^{12}CO 2–1/1–0 and 3–2/1–0 ratios but much higher ^{12}CO/^{13}CO ratios.

M 51: in the escape probability analysis of CO and ^{13}CO ratios in M 51, we discarded solutions leading to temperatures below 12.5 K and densities below $10^3\,{\rm cm}^{-3}$ as unphysical. Since the CO J = 3–2 is strong at all positions, densities and temperatures must be higher.

The CO 3–2/2–1 ratios are ∼0.8 at all positions in M 51, significantly higher than in M 83. This indicates higher densities than found in M 83. Indeed, the escape probability analysis finds densities between 3×10^3 and $3 \times 10^4\,{\rm cm}^{-3}$. The ^{12}CO/^{13}CO ratios agree with this solution for low temperatures of ∼12 K. However, the observed CO 2–1/1–0 ratios are too low to agree with this solution. Neither the temperatures nor the densities are well constrained, and minimum chi squared values are high. This shows the short coming of a one-component model even when trying to model only the three lowest rotational CO transitions. And it is in fact in agreement with the finding of Garcia-Burillo et al. (1993b) who used the lowest two transitions of ^{12}CO and ^{13}CO and couldn't find a set of $T_{\rm kin}$ and $n_{\rm loc}$ fitting simultaneously the line ratios for the arms and for the central position.

4.2. PDR analysis

To further constrain the physical conditions at the observed positions in M 83 and M 51, we compare the observed line intensity ratios with the results of the model for Photon Dominated Regions (PDRs) by Kaufman et al. (1999); Tielens & Hollenbach (1985). The physical structure is represented by a semi-infinite slab of constant density, which is illuminated by FUV photons from one side. The model takes into account the major heating and cooling processes and incorporates a detailed chemical network. Comparing the observed intensities with the steady-state solutions of the model, allows for the determination of the gas density of H nuclei, n, and the FUV flux, G_0, where G_0 is measured in units of the Habing (1968) value for the average solar neighborhood FUV flux, 1.6×10^{-3} ergs cm^{-2} s^{-1}. As has been pointed out in detail by Kaufman et al. (1999) in their Sect. 3.5.1 and several other authors, the application of these models to extragalactic observations is not straightforward since individual molecular clouds are not resolved in single-dish observations and several phases of the ISM are therefore observationally coexistent within each beam. The additional many degrees of freedom in the parameter space for more complex models, however, are ill constrained by the few observed, beam-averaged line ratios. Hence, simplistic models, e.g. with only a single source component, are used to at least derive average properties of the complex sources. Nevertheless, it is possible to obtain some insight into the spatial structure and the local excitation conditions, as we will show.

4.2.1. [C II] emission from the ionized and neutral medium

Carbon has a lower ionization potential (11.26 eV) than hydrogen, so that [C II] emission arises not only from photon dominated regions, but also from the ionized phases of the ISM and from the diffuse neutral medium traced by H I.

Analyzing the Milky Way FIR line data obtained with FIRAS/COBE (Fixsen et al. 1999), Petuchowski & Bennett (1993) argue that slightly more than half the [C II] emission in the Milky Way arises from PDRs, the remainder from the extended low density warm ionized medium or diffuse ionized medium (DIM), and an insignificant portion from the ordinary cold neutral medium (CNM).

[C II] emission from the ionized medium. Here, we use the observed [N II](122 μm) and [C II] lines, to estimate the fraction of [C II] originating from the ionized medium. However, a thorough analysis would need more FIR emission line data from the ionized medium, in particular the [N II](205 μm) line, to discriminate the relative importance of the different phases of the ionized medium (Bennett et al. 1994). Extragalactic observations of the [N II](205 μm) are however very rare to date (Petuchowski et al. 1994).

The components of the ionized phase of the ISM which contribute to the [C II] emission are dense HII regions ($n_{\rm e} \geq 100\,{\rm cm}^{-3}$) and the diffuse ionized medium (DIM) ($n_{\rm e} \sim 2\,{\rm cm}^{-3}$) (Heiles 1994).

The fraction of [C II] stemming from H II regions depends strongly on the electron density of the ionized medium. Carral et al. (1994) showed that upto 30% of [C II] stems from H II regions when electron densities exceed $100\,{\rm cm}^{-3}$. For dense HII regions ($n_{\rm e} \gg n_{\rm cr}$), model calculations suggest [C II]/[N II] = 0.28(C/N)$_{\rm dense}$ (Rubin 1985) where (C/N)$_{\rm dense}$ is the abundance ratio. The Galactic abundance ratio found in dense H II regions is 3.8 (Rubin et al. 1988, 1993). We thus expect to find an intensity ratio of

$$[{\rm C\,II}]/[{\rm N\,II}]_{\rm ion,H\,II} = 1.1. \quad (1)$$

Observations of radio free-free emission suggest that the DIM has typical volume densities of $n_{\rm e} \sim 2$ cm^{-3} (Mezger 1978) and temperatures of $T_{\rm e} = 4000$ K (Mueller et al. 1987). Densities are thus considerably lower than the critical densities of 310 cm^{-3} for the [N II](122) line and $50\,{\rm cm}^{-3}$ for the [C II](158) line (Genzel 1991). In this limit, the total power emitted in the collisionally excited fine-structure lines is simply the photon energy times the upward collision rate, as

given by Heiles (1994). The resulting ratio of intensities is: [C II]/[N II](122) = $3.05(C/N)_{diff}$. Galactic absorption line measurements of diffuse gas give $(C/N)_{DIM} = 1.87$ (Sofia et al. 1997; Meyer et al. 1997), which implies an expected intensity ratio of

$$([C\,II]/[N\,II](122))_{ion,DIM} = 5.7. \quad (2)$$

The preceeding section follows basically the arguments of MKH01 and Contursi et al. (2002).

The metallicities, parametrized by the oxygen abundances, have been found to be only slightly supersolar in M 83 and M 51. Zaritsky et al. (1994) find (O/H) abundances of 1.5×10^{-3} and 1.9×10^{-3} respectively, at 3 kpc galacto-centric distance, from visual spectra of H II regions, which is about a factor 3 higher than the solar metallicity of 0.46×10^{-3} (Asplund et al. 2004). Abundance gradients with radius are found to be shallow in M 83 and M 51 (Zaritsky et al. 1994). More recent observations with ISO/LWS and modelling of the CCM10 H II region of M 51 by Garnett et al. (2004) indicate instead that the (O/H) abundances are about a factor of 2 less, i.e. roughly solar. In addition, Garnett et al. (1999) showed that the (C/N) abundance ratio, which is of interest for the [C II]/[N II] ratio discussed here, is independent of metallicity in both normal and irregular galaxies. We therefore use Galactic abundances to estimate the intensity ratios in M 83 and M 51. For the Milky Way, Heiles (1994) have estimated that [N II] originates predominantly from the DIM, contributing ~70%. This was derived from the observed [N II](122)/[N II](205) ratio using photo ionization models. However, the [N II](205) line has not yet been observed in M 83 and M 51. We therefore use Eqs. (2) and (1), assuming that [N II] stems solely from H II regions, or alternatively, solely from the DIM.

Next, we can then derive the fraction of [C II] emission originating from PDRs:

$$[C\,II]_{PDR} = [C\,II]_{obs} - \left(\frac{[C\,II]}{[N\,II]}\right)_{ion} \times [N\,II](122)_{obs}. \quad (3)$$

The ratios of observed [C II] versus [N II] intensities vary between 3.6 and 7.4 at the six positions observed in M 83 and M 51 (Table 8). Garnett et al. (2004) found a higher ratio of 11.8 at the CCM 10 position in M 51.

The ratios found in M 83 and M 51 lie at the low end of the ratios MKH01 found in the sample of 60 unresolved normal galaxies studied. They show a mean ratio of 8 and a scatter between 4.3 and 29. Contursi et al. (2002) observed ratios of more than 7.7 in NGC 6946 and ratios of greater than 4 and 10 in NGC 1313. Higdon et al. (2003) found ratios between ≥2.6 and 20 in M 33.

If the [N II] emission originates only from the diffuse ionized medium, then the major fraction of [C II] arises from this phase, and only a small fraction from PDRs (Table 8). The observed [C II]/[N II] is ≤5.8 at 3 positions, including the two nuclei, which would indicate that no [C II] emission at all arises from PDRs. This is however unrealistic, since the emission of the [O I](63 μm) line, stemming from warm, dense PDRs, is strong compared to the [C II] lines, especially in the nuclei (Table 3). For this reason, we discard this solution.

Assuming, on the other hand, that the fraction of [C II] from the ionized medium and all [N II] emission stem only from the dense H II regions, then a fraction of only 15% to 30% of [C II] originates from this phase (Eq. (3)), while 70% to 85% of the observed [C II] emission then stems from PDRs. We prefer this solution and use it in the PDR analysis discussed below. In an ISO/LWS study of star-forming regions in M 33, Higdon et al. (2003) have recently used FIR lines of the ionized medium, i.e. [O III](88 μm), [O III](52 μm) and others to estimate the electron densities and other parameters of the emitting gas, estimating that between 7% and 47% of [C II] stems from H II regions, for their sample of positions. They conclude that the DIM is not needed to explain the observations.

[C II] emission from the diffuse neutral medium. The predicted [C II] emission from the atomic gas in general, for many galactic nuclei, has been found to be far too weak to account for the observed [C II] emission (Stacey et al. 1991) because the density is not high enough to appreciably excite the [C II] emission at the measured H I column densities. This view was confirmed by (Carral et al. 1994) who conducted a detailed study of FIR cooling lines of NGC 253 and NGC 3256. Both in M 51 and in M 83, no large-scale correlation between H I emission and that of [C II] is seen, indicating again that [C II] does not trace the diffuse neutral medium (Nikola et al. 2001; Crawford et al. 1985).

Nikola et al. (2001) used H I column densities (Tilanus & Allen 1991; Rots et al. 1990) to derive the contribution to the [C II] emission in M 51, assuming the same range of temperatures, densities, and ionization fractions for the warm and cold neutral medium (WNM, CNM) as have been found for the Milky Way. They find that the contribution of the WNM is negligible for most of the M 51 disk except the northwest, which was not studied here. The contribution of the CNM is estimated to be less than 10%−20% in all regions but the northwest.

We have thus not corrected the [C II] emission for a possible contribution from the diffuse neutral medium.

4.2.2. The infrared continuum and the FUV field

The stellar FUV photons heat the molecular gas and dust which subsequently cools via the FIR dust continuum and, with a fraction of less than ~1% (Stacey et al. 1991), MKH01 via [C II], [O I](63), and other cooling lines. To the extent that filling factors are 1 and other heating mechanisms like cosmic ray heating can be neglected, the observed TIR continuum intensity should equal the modelled FUV field. This is also expected if a constant fraction of FUV photons escape without impinging on cloud surfaces.

The PDR model of Kaufman et al. (1999) assumes a semi-infinite slab illuminated from one side only. For the extragalactic observations described here, we however have several PDRs within one beam and the clouds are illuminated from all sides. Hence, the optically thin total IR intensity stems from the near and far sides of clouds. Here, this is taken into account by dividing the observed TIR by 2 (Kaufman et al. 1999): $TIR_c = TIR/2 = 2.3 \times FIR/2$ (cf. Sect. 2.4). While this

Table 7. Physical parameters at the observed positions M 83 and M 51, derived from fitting the observed intensity ratios to PDR models of Kaufman et al. (1999). Column (2) gives the galacto-centric distance. Columns (3) and (4) list the fitted local densities and FUV fields together with the corresponding surface temperature (Col. (5)) and the minimum chi squared (Col. (6)). The filling factor $\phi_{\rm UV} = G_{0,\rm obs}/G_0$ reflects the ratio of $\rm TIR_c$ to the best fitting FUV field G_0. $\phi_{\rm A}^{\rm CI}$ is the area filling factor of the [C I] emitting regions, i.e. the ratio of observed [C I] intensity vs. that of the best fit model, corrected for beam and velocity filling (see text).

($\Delta\alpha$,$\Delta\delta$)	$R_{\rm gal}$	n	$\log(G_0)$	$\rm T_s$	χ^2	$\log(\rm G_{0,obs})$	$\phi_{\rm UV}$	$\phi_{\rm A}^{\rm CI}$
[″, ″]	[kpc]	[10^4cm^{-3}]		[K]				
(1)	(2)	(3)	(4)	(5)	(6)	(7)	(8)	(9)
M 83:								
(0, 0)	0.00	4.0	1.50	76.	2.8	2.16	4.57	0.019
(−80, −72)	1.93	4.0	1.50	76.	12.9	1.51	1.03	0.011
(89, 38)	1.76	4.0	1.50	76.	15.3	1.47	0.94	0.010
M 51:								
(0, 0)	0.00	4.0	1.25	66.	3.2	1.88	4.31	0.013
(72, 84)	5.40	4.0	1.25	66.	5.2	1.32	1.17	0.016
(−84, −84)	5.77	4.0	1.25	66.	14.1	1.19	0.88	0.009

correction holds exactly only for finite plane parallel slabs illuminated from both sides, it is a good first approximation. The corrected TIR can then be used to derive the corresponding FUV intensity via $G_{0,\rm obs} = \rm TIR_c 4\pi/(2 \times 1.6 \times 10^{-3})$ ergs cm^{-2} s^{-1}. Following the arguments of Kaufman et al. (1999), the additional factor 2 takes into account equal heating of the grains by photons outside the FUV band, i.e. by photons of $h\nu < 6$ eV. We find a variation by one order of magnitude, $15 < G_{0,\rm obs} < 144$ (Table 7, Fig. 4).

4.2.3. First estimates of FUV field and density

The two intensity ratios $\rm [O\,I](63)/[C\,II]_{PDR}$ and $\rm ([O\,I](63)+[C\,II]_{PDR})/TIR_c$, of the two major PDR cooling lines and the continuum, have been used extensively to derive the density and FUV field of the emitting regions (e.g. MKH01). Since [O I](63) and [C II] are the dominant coolants, the latter ratio is a good measure of the photoelectric heating efficiency ϵ (e.g. Kaufman et al. 1999). The former ratio measures the relative importance of [C II] vs. [O I](63) cooling. For high FUV fields and high densities, the ratio becomes larger than one (Kaufman et al. 1999).

In M 83 and M 51, the intensity ratio $\rm [O\,I](63)/[C\,II]_{PDR}$ varies only slightly between 0.8 and 1.3 (Table 8b). The heating efficiency varies between ∼0.25 and 0.36% at the outskirt positions while it drops to below 0.21% in the centers.

The values which we find in M 83 and M 51 lie within the range covered by MKH01, who find heating efficiencies ranging between ∼0.3% and ∼0.05% for the 60 galaxies studied, while the [O I]/[C II] ratios range between 0.3 and ∼10. Though the scatter is large, the heating efficiency tends to be high >0.15% for [O I]/[C II] ratios of less than 2. The $\rm [O\,I](63)/[C\,II]_{PDR}$ ratios found in M 83 and M 51 agree roughly with the average value found by MKH01, while the heating efficiencies in M 83 and M 51 span the average value of MKH01 upto the highest efficiencies found by them.

MKH01 corrected the observed [C II] emission by roughly 50% when taking into account the contribution from the ionized medium, based on the Milky Way results. Here, we corrected by only 15% to 30% (Table 8b). This uncertainty in how best to correct the [C II] fluxes needs to be considered when comparing the derived heating efficiencies and [O I]/[C II] ratios.

The small scatter of the observed two ratios at the 6 positions in M 83 and M 51 indicates that the emitting gas has similar physical properties. Comparison with the results of the Kaufman PDR model shows that two solutions exist (Fig. 3). The data can be reproduced either by high FUV fields at low densities or by low FUV fields and high densities. The high-G_0 solution indicates $2.5 \le \log(n/\rm cm^{-3}) \le 3.2$ and $2.4 \le \log G_0 \le 3$. As we will show, the low-G_0 solution is less plausible. It indicates rather high densities of $4.3 \le \log(n/\rm cm^{-3}) \le 4.5$ and low FUV fields of $0.1 \le \log G_0 \le 0.5$. In this case, the observed [C II] intensities are more than three orders of magnitude larger than the modelled intensities which would indicate that many PDR slabs along the lines of sight. Since the optical depth of the [C II] line in the line centers is expected to be about one (Kaufman et al. 1999), this scenario is discarded. This argument also holds when velocity filling is taken into account, since the velocity filling factor is <40 at all positions, as discussed below. We note that Higdon et al. (2003) in their analysis of ISO/LWS data of M 33, also discussed the two possible PDR solutions, and, following a different line of reasoning, also preferred the high-G_0 solution.

The n, G_0 values we find for the high-G_0 solution, agrees with the average values found by MKH01 who also exclude the low-G_0 solution. Their sample of 60 unresolved galaxies covers a slightly larger range of values: $2 < \log(n/\rm cm^{-3}) < 4.25$ and $2.5 < \log G_0 < 5$. Our values also agree with the average value found in NGC 6946 by Contursi et al. (2002).

4.2.4. PDR model fitting of five line ratios

In order to determine with greater confidence the densities and UV fluxes which can explain the intensity ratios, we have performed a χ^2 fitting of the observed 5 line intensity ratios

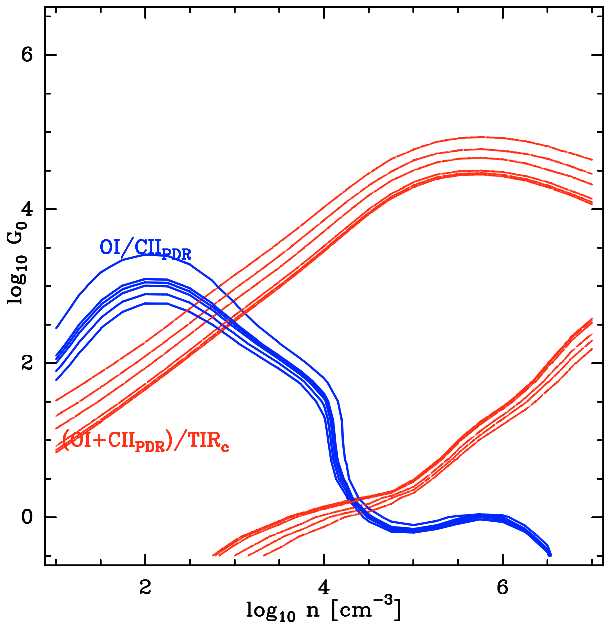

Fig. 3. Comparison of the observed intensity ratios [O I](63 μm)/[C II]$_{PDR}$ and ([O I](63 μm)+[C II]$_{PDR}$)/TIR$_c$ with PDR models (Kaufman et al. 1999) at the six positions in M 83 and M 51.

[C II]$_{PDR}$/[C I](1–0), [C I](1–0)/CO(3–2), CO(3–2)/CO(1–0), [C II]/CO(3–2), and, [O I](63)/[C II]$_{PDR}$ relative to the predictions of the PDR model by Kaufman et al. (1999):

$$\chi^2 = \frac{1}{4-2}\sum_{i=1}^{5}\left(\frac{R_i^{obs}-R_i^{mod}}{\sigma_i}\right)^2$$

with the observed and modelled ratios R_i^{obs} and R_i^{mod}, and the error σ_i which is assumed to be 20% for all ratios[3]. In Fig. 4 each panel shows the observed line intensity ratios and the calculated reduced χ^2 in greyscale for each observed position in M 83 and M 51. Table 7 summarizes the local density (n) and FUV radiation field (G_0) at the position of minimum reduced χ^2 corresponding to the best fit models thus identified. The [C I](1–0)/CO(3–2) and the CO(3–2)/(1–0) ratios are excellent tracers of the local densities, almost independent of G_0 for $G_0 > 10$. The sensitivity of [C II] on the FUV field is reflected by the line ratios which include [C II]. The combination of all these ratios therefore allows, in principle, to deduce n and G_0.

Densities. Though the quality of the fit varies strongly between the six positions, the best fitting FUV field and density are almost identical: $n = 10^4$ cm^{-3} and $18 < G_0 < 32$ (Table 7). Model surface temperatures are ~70 K. This is slightly lower than the upper energy level of [C II](158), $E_{up}/k = 92$ K, and much lower than the corresponding level of [O I](63), $E_{up}/k = 228$ K. Since the critical densities of the two [O I] lines for collisions with H are also high, $>10^5$ cm^{-3}, the [O I] lines are subthermally excited. Nevertheless, gas cooling is dominated by [C II] and [O I], contributions from H_2 or Si, covered by ISO/SWS, are negligible at these low temperatures. The best fitting density agrees within a factor of 3 with the local densities derived above via simple radiative transfer analysis, using only the ^{12}CO and ^{13}CO line ratios (Table 6).

[3] There are two degrees of freedom since we use four independent line ratios to fit two parameters.

Table 8. FIR line ratios after correcting the observed [C II] intensities for emission from the ionized medium. We study two cases: the emission of [C II] from the ionized medium originates entirely **a)** from the diffuse medium, and **b)**, that the emission arises entirely from dense H II regions. Also shown is the intensity ratio ϵ of the two major cooling lines of PDRs ([O I](63)+[C II]$_{PDR}$) vs. the observed TIR continuum.

$\Delta\alpha/\Delta\delta$	$\frac{[C\,II]_{obs}}{[N\,II](122)}$	$\frac{[C\,II]_{PDR}}{[C\,II]_{obs}}$	$\frac{[O\,I](63)}{[C\,II]_{PDR}}$	ϵ [%]
a) [N II] only from the DIM:				
M 83:				
0, 0	5.8	0.02	57.41	0.12
−80, −72	7.3	0.22	3.18	0.22
89, 38	5.7	0.00	–	0.17
M 51:				
0, 0	3.6	0.00	–	0.08
72, 84	7.3	0.22	3.59	0.16
−84, −84	7.4	0.23	3.78	0.21
b) [N II] only from H II-regions:				
M 83:				
0, 0	5.8	0.81	1.31	0.21
−80, −72	7.3	0.85	0.83	0.36
89, 38	5.7	0.81	0.99	0.35
M 51:				
0, 0	3.6	0.69	1.06	0.16
72, 84	7.3	0.85	0.91	0.25
−84, −84	7.4	0.85	1.02	0.33

UV filling factor. At the four spiral arm positions, the total infrared continuum agrees perfectly with the best fitting FUV field (Table 7), which is an independent confirmation of the validity of the PDR analysis using the five line ratios. The active center regions of M 83 and M 51 show filling factors of ~4, indicating that other sources than PDRs heat the dust leading to the high observed TIR intensities, e.g. massive protostars.

Quality of the fits. The minimum reduced chi squared of the 4 independent ratios lie between 3 and 15 at all positions (Table 7). While the two nuclei and the NE-spiral arm position of M 51 show χ^2 of better than 5, the other three spiral arm positions show rather poor χ^2 values of 13–15.

Inspection of Fig. 4 shows that, at the latter three positions, the [C II]$_{PDR}$/[C I] ratio indicates higher FUV fields than the best fitting solution. In addition, Figure 4 also shows that the CO 3–2/1–0 line ratios indicates systematically lower densities than the observed [C I]/CO 3–2 ratios. This holds to varying degrees for all positions and for $G_0 > 10$. By assuming [C I] intensities which are a factor 2 higher, the quality of the fit is considerably improved, while the best fitting G_0 and density stay constant at all positions. At (−80, −72) in M 83 for example, the χ^2 is improved from 12.9 to 3.4. This indicates that

the beam filling factors of the [C I] emission, derived from the CO 2–1 data (Table 5), are too small, i.e. [C I] is more extended than CO.

We also conclude that our results are consistent with the assumption that only the dense ionized medium contributes to the [C II] emission. There is no need for an extended diffuse component.

Overall, the observed five ratios cannot be well fitted with a single plane-parallel PDR model of constant density at any of the positions. This is not surprising as the excitation requirements of the various tracers collected here vary widely. Especially, the critical densities vary between $5 \times 10^2\,\mathrm{cm}^{-3}$ for the lower [C I] transition and $5 \times 10^5\,\mathrm{cm}^{-3}$ for the [O I] 63 μm transition. Any density gradients in the emitting medium may thus lead to the above discrepancies with a single PDR model depending also on the chemical and temperature structure. In addition, the large difference between local densities derived here and beam averaged densities of more than three orders of magnitude (Table 6) shows that the emitting volume must be filled with very small but dense structures. From many Galactic observations, it is expected that these structures show a spectrum of masses, adding to the complexity ignored here.

Absolute intensities. When comparing the observed intensities with the model results, the velocity filling also has to be taken into account. The observed [C I] line widths $\Delta v_{\rm obs}$ range between 30 and 130 km s^{-1} *FWHM* (cf. Sects. 3.1 and 3.2) measuring the dispersion of clouds within the beam for these extragalactic observations. On the other hand, the microturbulent velocity dispersion δ_v of the gas of one PDR model is set to 1.5 km s^{-1} (Kaufman et al. 1999), corresponding to a Gaussian *FWHM* $\Delta v_{\rm mod}$ of 3.5 km s^{-1} as is typical for individual Galactic clouds. To calculate the [C I] area filling factors (Table 7), we divided the observed [C I] intensities by the predicted [C I] intensity from the best fitting model, corrected for beam (Table 5) and velocity filling, viz.,

$$\Phi_{\rm A}^{\rm CI} = \frac{\left([\mathrm{CI}]_{\rm obs} \times \Phi_{\rm B}^{80/10}\right)}{[\mathrm{CI}]_{\rm mod}} \times \frac{\Delta v_{\rm mod}}{\Delta v_{\rm obs}}.$$

[C I] emission fills only a few percent of the 80″ beam, the derived area filling factors vary between $(1-2)\times10^{-2}$ (Table 7), consistent with the low volume filling factors described above.

5. Summary

We have studied all major submillimeter and far infrared cooling lines together with the dust total infrared continuum at the center positions of the two galaxies M 83 and M 51 and at four spiral arm positions.

We observed [C I] 1–0 at the six positions at 10″ resolution. Complementary [C II], [O I](63), and [N II](122) data were obtained from ISO/LWS at 80″ resolution. CO maps of the lowest three transitions were obtained from the literature and smoothed to the ISO/LWS resolution. We also obtained pointed ^{13}CO 1–0 and 2–1 data at all positions. In order to allow a comparison of all these data, the [C I] and ^{13}CO data were scaled with beam filling factors derived from the ^{12}CO data. For completeness, we also obtained the total far-infrared continuum intensities from HIRES/IRAS 60 μm and 100 μm data.

- Integrated intensities peak in the two centers. However, M 83 is much more centrally peaked than M 51 as seen in CO and [C I] as is already seen in the spectra (Figs. 1, 2). This is seen even more drastically in the drop of [C I] luminosities with galacto-centric distance. In M 83, luminosities drop by more than one order of magnitude over ∼2 kpc, while in M 51, they drop by only a factor of ∼4 over ∼6 kpc. Obviously, this analysis should be refined by more observations of [C I] at different radii.
- The ^{12}CO 3–2/1–0 line ratios lie below 0.6 at all positions, indicating subthermal excitation of the 3–2 line, i.e. densities are less than $10^5\,\mathrm{cm}^{-3}$. This is confirmed by more detailed analysis using escape probability and PDR models. The former homogeneous models indicate densities between 3×10^3 and $3 \times 10^4\,\mathrm{cm}^{-3}$ from CO and ^{13}CO line ratios.
- We estimated the fraction of observed [C II] emission originating from the ionized medium by using the [N II] 122 μm data which traces only this medium. In the absence of additional data, which would allow us to seperate the contributions from the different phases of the ionized medium, we argue that dense H II regions are the primary source of [N II] emission. These emit 15% to 30% of the observed [C II] emission while the remainder stems from PDRs.
- The gas heating efficiency was calculated from the ratio of the two major gas coolants [O I] at 63 μm and $[\mathrm{C\,II}]_{\rm PDR}$ at 158 μm versus the total infrared intensity. The efficiency is low in the centers showing ratios of $(1.6-2.1)\times10^{-3}$, while the outer positions show higher ratios of $(2.5-3.6)\times10^{-3}$. The latter efficiencies lie at the high end of efficiencies observed by MKH01 in a sample of 60 unresolved normal galaxies.
- We fitted the observed line intensity ratios $[\mathrm{C\,II}]_{\rm PDR}$/[C I](1–0), [C I](1–0)/CO(3–2), CO(3–2)/CO(1–0), [C II]/CO(3–2), and [O I](63)/$[\mathrm{C\,II}]_{\rm PDR}$ to the predictions of the PDR model of Kaufman et al. (1999). The best fits yield densities of $10^4\,\mathrm{cm}^{-3}$ and FUV fields of $\sim G_0 = 20-30$ times the average interstellar, almost constant at the six positions studied here at 80″ resolution. This finding may be a selection effect, since we selected the four outer positions for their high star forming activity. More observations of other less prominent positions are needed to study variation of physical parameters over the galaxy surfaces.
- Filling factors vary significantly between the center positions and the outer positions in both galaxies. The filling factor $\phi_{\rm UV}$ derived from the FUV field calculated from the observed total infrared intensity versus the fitted G_0 lies at 1 at the spiral arm positions, with a scatter of less than 20%. In contrast, the nuclei show ratios of ∼4–5. The density contrasts within the emitting gas must be high, given the local densities of $10^4\,\mathrm{cm}^{-3}$ and the average densities, derived from CO column densities, of less than $1\,\mathrm{cm}^{-3}$, leading to very low volume filling factors. In accordance, the

area filling factors of the [C I] emission are less than 2% at all positions.
- The reduced χ^2 values lie between 3 and 5 at three positions, including the two nuclei, while the fits are worse at the three other positions, which show $\chi^2 = 13$–15. It is shown that the fits can be significantly improved by assuming that [C I] emission is more extended.

While the present analysis led to the results listed above, it needs to be refined with new data and improved modelling. The assumption that all gas tracers have the same filling factors may not be justified. We find indications that [C I] is more extended than CO 2–1. Clearly, maps of [C I] at 10″ resolution filling the ISO/LWS 80″ beam would be needed to verify this conclusion. A related question is the nature of the interclump medium and whether it can be ignored when interpreting the submm/FIR emission. The fraction of [C II] emission from the different phases of the ionized medium has been addressed here by assuming that all emission stems from the dense ionized medium. While this is consistent with the PDR modelling, it probably is an oversimplification. Observations of the [N II] line at 205 μm would allow us to refine this analysis. Such observations will become possible with a new generation of submm telescopes and receivers operating at high altitudes. In this regard, modelling neads to include the ionized medium. Improved PDR models need to consider a distribution of clouds within each beam, following mass and size distribution laws.

Acknowledgements. We thank Steve Lord for valuable discussions. We would like to thank the JCMT and the IRAM 30 m staff for providing excellent support during several long runs at the Mauna Kea and the Pico Veleta. We are greatful to Michael Dumke for providing us with HHT CO 3–2 and 4–3 M 51 data and Lucian Crosthwaite for NRAO CO 1–0 and 2–1 M 83 data. And we thank Jim Brauher, Steve Lord, and Alessandra Contursi for providing us with the ISO/LWS line fluxes of both galaxies. The James Clerk Maxwell Telescope is operated by the Joint Astronomy Centre on behalf of the Particle Physics and Astronomy Research Council of the United Kingdom, The Netherlands Organisation for Scientific Research, and the National Research Council of Canada. This work has benefited from research funding from the European Community's Sixth Framework Programme. We made use of the NASA IPAC/IRAS/HiRes data reduction facilities.

References

Aalto, S., Huettemeister, S., Scoville, N. Z., & Thaddeus, P. 1999, ApJ, 522, 165
Asplund, M., Grevesse, N., Sauval, A. J., Allende Prieto, C., & Kiselman, D. 2004, A&A, 417, 751
Aumann, H., Fowler, J., & Melnyk, M. 1990, AJ, 99, 1674
Bakes, E., & Tielens, A. 1994, ApJ, 427, 822
Bayet, E., Gerin, M., Phillips, T., & Contursi, A. 2004, A&A, 427, 45
Bennett, C. L., Fixsen, D. J., Hinshaw, G. G. H., et al. 1994, ApJ, 434, 587
Carral, P., Hollenbach, D. J., Lord, S. D., et al. 1994, ApJ, 423, 223
Carranza, G., Crillon, R., & Monnet, G. 1969, A&A, 1, 479
Contursi, A., Kaufman, M., Helou, G., et al. 2002, ApJ, 124, 751
Crawford, M., Genzel, R., Townes, C., & Watson, D. 1985, ApJ, 291, 755
Crosthwaite, L., Turner, J., Buchholz, L., Ho, P., & Martin, R. 2002, ApJ, 123, 1892
Dale, D. A., Helou, G., Contursi, A., Silbermann, N. A., & Kolhatkar, S. 2001, ApJ, 549, 215
de Vaucouleurs, G. 1979, AJ, 84, 1270
de Vaucouleurs, G., de Vaucouleurs, A., Corwin, H. J., et al. 1991, Third reference catalogue of bright galaxies (New York: Springer-Verlag)
Dumke, M., Nieten, C., Thuma, G., Wielebinski, R., & Walsh, W. 2001, A&A, 373, 853
Fixsen, D. J., Bennett, C. L., & Mather, J. C. 1999, ApJ, 526, 207
Frerking, M. A., Langer, W. D., & Wilson, R. W. 1982, ApJ, 262, 590
Garcia-Burillo, S., Guelin, M., Cernicharo, J., & Dahlem, M. 1992, A&A, 266, 21
Garcia-Burillo, S., Combes, F., & Gerin, M. 1993a, A&A, 274, 148
Garcia-Burillo, S., Guelin, M., & Cernicharo, J. 1993b, A&A, 274, 123
Garnett, D. R., Shields, G. A., Peimbert, M., et al. 1999, ApJ, 513, 168
Garnett, D. R., Edmunds, M. G., Henry, R. B. C., Pagel, B. E. J., & Skillman, E. D. 2004, AJ, 128, 2772
Genzel, R. 1991, in The Galactic Interstellar Medium, ed. W. Burton, B. Elmegreen, & R. Genzel (Berlin, Germany: Springer-Verlag), 280
Gerin, M., & Phillips, T. 2000, ApJ, 537, 644
Gry, C., Swinyard, B., Harwood, A., et al. 2003, The ISO Handbook, Vol. III. LWS – The long wavelength spectrometer (ISO Data Centre: ESO)
Habing, H. 1968, Bull. Astr. Inst. Netherlands, 19, 421
Handa, T., Nakai, N., Sofue, Y., Hayashi, M., & Fujimoto, M. 1990, PASJ, 41, 1
Heiles, C. 1994, ApJ, 436, 720
Helou, G., Khan, I., Malek, L., & Boehmer, L. 1988, ApJ, 68, 151
Higdon, S. J. U., Higdon, J. L., van der Hulst, J. M., & Stacey, G. J. 2003, ApJ, 592, 161
Ho, L., Fillipenko, A., & Sargent, W. 1997, ApJ, 112, 315
Israel, F. P. 2005, Ap&SS, 295, 171
Israel, F. P., & Baas, F. 2001, A&A, 371, 433
Israel, F. P., & Baas, F. 2002, A&A, 383, 82
Israel, F. P., & Baas, F. 2003, A&A, 404, 495
Kaufman, M., Wolfire, M., Hollenbach, D., & Luhman, M. 1999, ApJ, 527, 795
Keene, J. 1995, in The physics and chemistry of the interstellar medium, ed. G. Winnewisser, & G. C. Pelz (Berlin: Springer)
Kenney, J., & Lord, S. 1991, ApJ, 381, 118
Kennicutt, R., Armus, L., Bendo, G., & Calzetti, D. 2003, PASP, 115, 928
Kohno, K., Kawabe, R., Tosaki, T., & Okumura, S. 1996, ApJ, 461, 29
Leech, K. J., Völk, H. J., Heinrichsen, I., et al. 1999, MNRAS, 310, 317
Lord, S., & Kenney, J. 1991, ApJ, 381, 130
Lundgren, L., Olofsson, H., Wiklind, T., & Rydbeck, G. 2004a, A&A, 422, 865
Lundgren, L., Wiklind, T., Olofsson, H., & Rydbeck, G. 2004b, A&A, 413, 505
Malhotra, S., Kaufman, M., Hollenbach, D., et al. 2001, ApJ, 561, 766
Matsushita, S., Kohno, K., Vila-Vilaro, B., Tosaki, T., & Kawabe, R. 1998, ApJ, 495, 267
Matsushita, S., Kohno, K., Vila-Vilaro, B., Tosaki, T., & Kawabe, R. 1999, Adv. Space Res., 23, 1015
Matsushita, S., Sakamoto, K., Kuo, C.-Y., et al. 2004, ApJ, 616, 55
Mauersberger, R., & Henkel, C. 1993, Rev. Mod. Astron., 6, 69

Mauersberger, R., Henkel, C., Walsh, W., & Schulz, A. 1999, A&A, 341, 256
Meyer, D. M., Cardelli, J. A., & Sofia, U. J. 1997, ApJ, 490, 103
Mezger, P. O. 1978, A&A, 70, 565
Mueller, P., Reif, K., & Reich, W. 1987, A&A, 183, 327
Nakai, N., Kuno, N., Handa, T. Y., & Sofue, Y. 1994, PASJ, 46, 527
Negishi, T., Onaka, T., Chan, K.-W., & Roellig, T. L. 2001, A&A, 375, 566
Neri, R., Genzel, R., Ivison, R. J., et al. 2003, ApJ, 597, 113
Nieten, C., Dumke, M., Beck, R., & Wielebinski, R. 1999, A&A, 347, 5
Nikola, T., Geis, N., Herrmann, F., et al. 2001, ApJ, 561, 203
Papadopoulos, P. P., Thi, W.-F., & Viti, S. 2004, MNRAS, 351, 147
Petitpas, G., & Wilson, C. 1998, ApJ, 503, 219
Petuchowski, S., & Bennett, C. 1993, ApJ, 405, 591
Petuchowski, S. J., Bennett, C. L., Haas, M. R., et al. 1994, ApJ, 427, L17
Pety, J., Beelen, A., Cox, P., et al. 2004, ApJ, 428, 21
Rand, R., Lord, S., & Higdon, J. 1999, ApJ, 513, 720
Regan, M., Thornley, M., Helfer, T., et al. 2001, ApJ, 561, 218
Rice, W., Lonsdale, C. J., Soifer, B. T., et al. 1988, ApJ, 68, 91
Rots, A., Crane, P., Bosma, A., Athanassoula, E., & van der Hulst, J. 1990, AJ, 100, 387
Rubin, R. H. 1985, ApJS, 57, 349
Rubin, R. H., Simpson, J. P., Erickson, E. F., & Haas, M. R. 1988, ApJ, 327, 377
Rubin, R. H., Dufour, R. J., & Walter, D. K. 1993, ApJ, 413, 242
Sakamoto, K., Okumura, S., Ishizuki, S., & Scoville, N. 1999, ApJ, 124, 403
Sakamoto, K., Matsushita, S., Peck, A., Wiedner, M., & Iono, D. 2004, ApJ, 616, L59
Sandage, A., & Tammann, G. 1975, ApJ, 196, 313
Sofia, U. J., Cardelli, J. A., Guerin, K. P., & Meyer, D. M. 1997, ApJ, 482, L105
Stacey, G., Geis, N., Genzel, R., et al. 1991, ApJ, 373, 423
Stoerzer, H., Stutzki, J., & Sternberg, A. 1996, A&A, 310, 592
Stutzki, J., & Winnewisser, G. 1985, A&A, 144, 13
Talbot, R. J., Jensen, E. B., & Dufour, R. J. 1979, ApJ, 229, 91
Thim, F., Tammann, G. A., Saha, A., et al. 2003, ApJ, 590, 256
Tielens, A., & Hollenbach, D. 1985, ApJ, 291, 722
Tilanus, R., & Allen, R. 1991, A&A, 244, 8
Tosaki, T., Hasegawa, T., Shioya, Y., Kuno, N., & Matsushita, S. 2002, PASJ, 54, 209
Tully, R. 1988, Nearby Galaxies Catalogue (Cambridge: University Press)
Walter, F., Carilli, C., Bertoldi, F., et al. 2004, ApJ, 615, 17
Weiss, A., Downes, D., Henkel, C., & Walter, F. 2005, A&A, 429, 25
Weiss, A., Henkel, C., Downes, D., & Walter, F. 2003, A&A, 409, 41
Wielebinski, R., Dumke, M., & Nieten, C. 1999, A&A, 347, 634
Zaritsky, D., Kennicutt, R. C., & Huchra, J. P. 1994, ApJ, 420, 87

Online Material

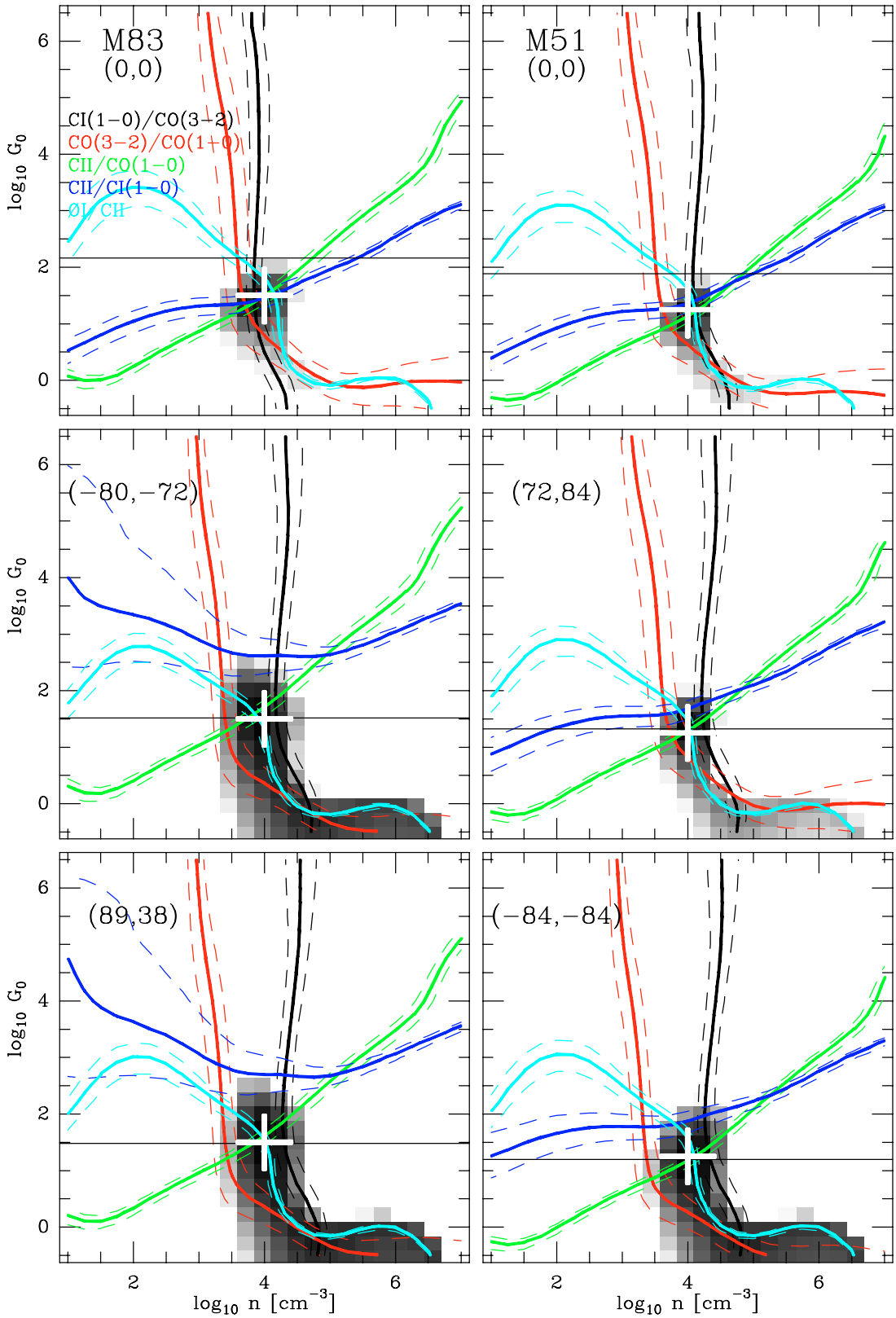

Fig. 4. Comparison of the observed line intensity ratios $[\mathrm{C\,II}]_{\mathrm{PDR}}/[\mathrm{C\,I}](1–0)$, $[\mathrm{C\,I}](1–0)/\mathrm{CO}(3–2)$, $\mathrm{CO}(3–2)/\mathrm{CO}(1–0)$, $[\mathrm{C\,II}]_{\mathrm{PDR}}/\mathrm{CO}(3–2)$ and $[\mathrm{O\,I}](63\ \mu\mathrm{m})/[\mathrm{C\,II}]_{\mathrm{PDR}}$ in M 83 and M 51 with PDR model calculations by Kaufman et al. (1999). The drawn contours correspond to the observed intensity ratios while the dashed contours are those for the 20% uncertainty. The greyscale images show the reduced χ^2 of the fit. The position of the minimum reduced chi squared is marked by a white cross (Table 7). The horizontal black line shows the FUV flux $G_{0,\mathrm{obs}}$ calculated from the observed $\mathrm{TIR_c}$ flux densities.